Pharmaceutical Research
https://doi.org/10.1007/s11095-023-03561-6

ORIGINAL RESEARCH ARTICLE

Selection of Silica Type and Amount for Flowability Enhancements via Dry Coating: Contact Mechanics Based Predictive Approach

Kuriakose T. Kunnath[1] · Siddharth Tripathi[1] · Sangah S. Kim[1] · Liang Chen[1] · Kai Zheng[1] · Rajesh N. Davé[1]

Received: 25 April 2023 / Accepted: 6 July 2023

Abstract

Purpose To investigate the effect of dry coating the amount and type of silica on powder flowability enhancement using a comprehensive set of 19 pharmaceutical powders having different sizes, surface roughness, morphology, and aspect ratios, as well as assess flow predictability via Bond number estimated using a mechanistic multi-asperity particle contact model.

Method Particle size, shape, density, surface energy and area, SEM-based morphology, and FFC were assessed for all powders. Hydrophobic (R972P) or hydrophilic (A200) nano-silica were dry coated for each powder at 25%, 50%, and 100% surface area coverage (SAC). Flow predictability was assessed via particle size and Bond number.

Results Nearly maximal flow enhancement, one or more flow category, was observed for all powders at 50% SAC of either type of silica, equivalent to 1 wt% or less for both the hydrophobic R972P or hydrophilic A200, while R972P generally performed slightly better. Silica amount as SAC better helped understand the relative performance. The power-law relation between FFC and Bond number was observed.

Conclusion Significant flow enhancements were achieved at 50% SAC, validating previous models. Most uncoated *very cohesive* powders improved by two flow categories, attaining *easy flow*. Flowability could not be predicted for both the uncoated and dry coated powders via particle size alone. Prediction was significantly better using Bond number computed via the mechanistic multi-asperity particle contact model accounting for the particle size, surface energy, roughness, and the amount and type of silica. The widely accepted 200 nm surface roughness was not valid for most pharmaceutical powders.

Keywords dry coating · flow enhancement · flowability prediction · hydrophobic or hydrophilic nano-silica · granular bond number

Introduction

Flowability is an important bulk-scale material property of dry powders that dictates several aspects of pharmaceutical tablet production, such as conveying, discharging, die filling, blending, and blend content uniformity [1–5]. Flowability is a major concern for finer powders (< 50 μm) since they are more cohesive as their interparticle adhesion force is much greater than the individual particle's weight [6, 7]. In addition to the nominal particle size, the powder cohesion and flowability are also influenced by many other factors, such as the particle material, size distribution, shape, morphology, surface roughness, surface energy, as well as environmental conditions, such as the relative humidity and temperature [7–11]. In part, since many factors could impact the powder flowability, there is a lack of a mechanistically based predictive method for a priori determination of how a

Highlights
- Flow improved by 1+ regimes via dry coating for all 19 APIs/excipients (5-200 mm).
- 50 %SAC silica (1 wt% or less) led to *optimal* flow (FFC) increase for all powders.
- Hydrophobic-R972P and hydrophilic-A200 silica perform well, R972P slightly better.
- The granular Bond number better predicts flowability/FFC than the particle size.
- Surface roughness is a dominant factor for flow, 200 nm value not universally valid.

✉ Rajesh N. Davé
dave@njit.edu

[1] New Jersey Center for Engineered Particulates, New Jersey Institute of Technology, Newark, NJ 07102, USA

Published online: 20 July 2023

pharmaceutical powder will flow or pack. Therefore, there have been attempts to develop data-driven empirical models to predict powder flow [12–20]. However, empirical models lack fundamental physics which governs particle behavior and therefore, there is a need for more fundamental approaches, for example, those that consider nondimensionalized parameters. Towards predictability of powder properties, a dimensionless measure of cohesion, granular Bond number, Bo_g, which is the ratio of the sum of cohesive forces to the body forces, also called the force ratio, has been the most preferred option [6, 21–24]. For uncharged dry powders devoid of appreciable moisture, it is essentially the ratio of particle-particle van der Waals force to particle weight. Generally, when $Bog < 1$, particles are non-cohesive and free-flowing; when $Bog >> 1$, they are cohesive and poorly flowing. Interestingly, most pharmaceutical materials having median particle size (d_{50}) of 50 μm or less, e.g., Ibuprofen50, Pharmatose350, Avicel-Ph-105, etc., exhibit poor flowability and as will be shown later, they indeed have $Bog >> 1$ and exhibit relatively poor flowability in terms their flow function coefficient (FFC) values, estimated via shear testing, for which physical interpretations are given in Table I [25].

There is an advantage of using Bo_g as a scaling parameter since it could account for variations in particle properties other than the size, such as their surface energy, surface roughness, etc., as has been shown for scaling as power law functions of Bo_g for fine particle aggregation [23], minimum bubbling velocity in fluidization [24], flowability [7, 26], particle packing [8, 27]. In most of these, using Bo_g is particularly advantageous when the flow is enhanced via dry coating, which could dramatically enhance flowability without altering the particle size, and will be considered in this paper [22, 28].

From a pragmatic perspective, it is crucial to be able to improve flowability in a reliable, predictable manner. Enhanced flowability and packing density are also beneficial since they could promote direct blend - direct compression (DB-DC) tableting, including continuous manufacturing (CM), provided the blends reach an adequate flowability and bulk density level [29–31]. An emerging approach for tackling poor flowability and processability of fine APIs is dry coating, a liquid-free method for reducing the cohesion of fine powders, leading to improved bulk powder properties, e.g., the flowability, agglomeration, packing density, fluidization, and dissolution [2, 22, 28, 32, 33]. In dry coating, the host powders, typically those which require flow enhancement, are covered with the guest particles, such as nano-silica, using mechanical means [28]. A significant advantage of dry coating is that it could also enhance powder blend properties and could promote direct compression tableting [34–37].

Table I Flow Classifications for Numerical Flow Function Coefficient (FFC) Values, as Given by Schulze [25]

FFC Value	Flow Classification
1–2	Very Cohesive
2–4	Cohesive
4–10	Easy-Flowing
> 10	Free-Flowing

The first question is how much silica to select for dry coating of a poorly flowing powder. This has been addressed partly via normalization of the silica amount in terms of percentage host particle surface area coverage (SAC), introduced by our group [22, 28]. This study highlights the benefits of employing commonsense normalization, mainly because the exemplary cohesive powders exhibit significant size disparities. The pharmaceutical industry commonly incorporates silica in terms of wt%. Therefore, numerous papers have adopted that approach, which may only be justifiable when examining a group of powders with relatively similar sizes [2, 26, 38]. In the present investigation, nearly twenty API and excipient powders, spanning median diameters from about 5 to over 200 μm are examined. Consequently, the surface area coverage (SAC) based on silica amount normalization is employed. The next question is if there are models that relate the silica SAC with dry coating effectiveness in terms of flow enhancement. The theoretical analysis and accompanying models have been proposed previously that explored the SAC range from 0 to 100% and demonstrated that the primary mode of a pair of host particle interaction shifts from host-host, guest-host, and guest-guest as the SAC increases, refer to Fig. 3 in [39]. Assuming a uniform size and distribution of spherical guest particles, it has been shown that in theory, SAC of ~30% assures guest-guest contacts [22, 23, 40].

Considering that outcome, silica amount normalization makes better sense than using fixed wt%, e.g., 1 wt% as done previously [26]. Further, although higher SAC values of up to 100% have been recommended in the past [32, 38], recent experimental and theoretical work has shown that in most cases, an excessive amount of silica may not be required [4, 41]. Instead, a host surface area coverage (SAC) of approximately 30–50% could be the most efficacious proportion [42]. Interestingly, Deng *et al.* concluded that there is a smoother transition from host-host to host-guest to guest-guest contact than that predicted by Chen [22]. Significant interparticle force reduction can be achieved with as little as 10% SAC [42]. Such results warrant a more detailed investigation of the appropriate silica SAC necessary for significant flow enhancements for a broad spectrum of pharmaceutical components, including both active pharmaceutical ingredients (API) and excipient powders. Therefore, that is a major objective of this paper.

An issue worthy of investigation is the type of silica to be used. The consensus has been that hydrophobic nano-silica is

superior to hydrophilic nano-silica in terms of flow improvement [36, 43–46]. However, the use of hydrophilic silica is also of great interest because it could promote improved tablet compaction [36, 47–50] and dissolution [36, 38, 51]. This paper addresses both the issue of the amount of silica and the type of silica by considering either hydrophobic (R972P) or hydrophilic silicas (A200) at several SAC levels for numerous commonly used pharmaceutical materials, both the APIs and excipients.

In what follows, first, the multi-asperity model [22], required to estimate Bo_g with and without dry coating, is presented. It can account for the effect of the silica type and amount and provide the rationale for normalizing the silica amount in terms of theoretical host particle surface area coverage. An accurate estimation of Bo_g is necessary for the examination of its expected power-law relationship with powder flowability for developing a predictive model. Therefore, the current limitations of the particle contact model are discussed, which may impact the accuracy of the flowability predictions. Next, the effect of the silica type, hydrophobic, R972P, and hydrophilic, A200, at SAC (0–100%) for a wide range of API and excipient host particles after nano-silica dry coating are experimentally assessed. Last, the applicability of Bo_g as a scaling parameter is tested for potentially predicting powder flowability as a power-law function of Bo_g, both before and after dry coating. This is done by incorporating powders with diverse particle sizes and shapes, providing a more inclusive test data set that could allow for more generalizable insights, which are unlikely to result from narrower data sets of the previous studies [26, 52].

Theory

Bo_g for dry powders is defined as the ratio of interparticle cohesive forces to particle weight, as described in Eq. 1.

$$Bo_g = \frac{F_{vdW}}{W_g} \tag{1}$$

Here, F_{vdW} is the interparticle cohesive force, and W_g is the particle weight. The calculation of particle weight (W_g) is straightforward, and is given in Eq. 2, where D is the median particle size and ρ_p is the powder's particle (true) density. The acceleration due to gravity (g) is approximated to be 9.8 m/s^2.

$$W_g = \frac{\pi}{6} D^3 \rho_p g \tag{2}$$

Interparticle cohesive force (F_{vdw}) may be computed using the multi-asperity model of Chen *et al.* [22], which accounts for contact forces between two spherical particles with evenly distributed surface asperities. In deriving this model, three guest particles are assumed to be placed on the vertices of an equilateral triangle between the two host spheres. The amount of guest particles required can be estimated by taking the projection of areas of all guest particles on the host particles [28] and may be estimated as:

$$SAC = \frac{N \times \frac{\pi d^2}{4}}{4\pi\left(\frac{d+D}{d}\right)^2} \times 100\% \tag{3}$$

Correspondingly, the required guest particles Wt% is:

$$Wt\% = \frac{\left(Nd^3\rho_d\right)}{\left(D^3\rho_D\right) + \left(Nd^3\rho_d\right)} \times 100\% \tag{4}$$

Where, N is the number of host particles estimated using the true density (ρ_D), mass, and size of the host (D) while d is the size of silica used and ρ_d it's true density.

The above equations may need to be modified for cases where the particles are non-spherical, have broad particle size distributions (PSDs), or their surfaces are macro-rough by casting these equations in terms of the host particle specific surface area (SSA) instead of the diameter.

The adhesive force between two coated particles can then be calculated by the Chen model [22].

$$F_{ad} = \frac{Ad}{4z_0^2} + \frac{A}{24\left(\sqrt{\left(1+\frac{d}{D}\right)^2 - \frac{1.21d^2}{SAC*D^2}} - 1\right)^2 * D} \tag{5}$$

Here, A is the Hamaker constant, D is the diameter of the host particle, d is the diameter of the guest particle, z_0 is the default distance between two surfaces in contact. The Hamaker constant (A) can be calculated using Eq. 6, where D_0 is the cut-off distance (0.165 nm) and γ_d is the dispersive surface energy.

$$A = 24\pi {D_0}^2 \gamma_d \tag{6}$$

It can be observed from Eq. 5 that cohesion force is a function of SAC, wherein the cohesion force decreases with an increase of SAC, resulting in three contact regimes, i.e., the Host-Host, Guest-Host, and Guest-Guest contact regime. The Host-Host regime occurs at very low surface coverage. The guest particles do not have any effect on the adhesion force reduction because the space between neighboring guest particles on the surface of the respective host particles is so large that the host particles contact each other directly. As the concentration of guest particles increases, the direct contact and hence adhesion

Table II Manufacturers, Median Particle Sizes (d_{50}), Sauter Mean Diameters ($d_{3,2}$), Particle (True) Densities (ρ_p), and Dispersive Surface Energies (γ_d) of the APIs used in this study

Material	Manufacturer	d_{50} (μm)	$d_{3,2}$ (μm)	ρ_p (kg/m^3)	γ_d (J/m^2)
micronized Acetaminophen (mAPAP)	Changshu Huagang Pharmaceutical Co., Ltd. China	7.31 ± 0.88	4.82 ± 0.21	1290	46.38
coarse Acetaminophen (cAPAP)	Mallinckrodt, Inc., USA	23.25 ± 1.1	17.54 ± 0.36	1290	40.86
Ibuprofen 50 (Ibu50)	BASF, USA	52.76 ± 1.6	32.20 ± 0.88	1120	38.92
Ascorbic Acid (AA)	Ruger, USA	224.28 ± 2.6	123.35 ± 0.92	1650	41.00
Fenofibrate (FNB)	Jai Radhe Sales, INDIA	6.82 ± 0.48	4.52 ± 0.10	1263	39.50
Griseofulvin (GF)	Lecto Medical, USA	10.56 ± 0.45	6.37 ± 0.08	1430	39.70
Itraconazole (ITZ)	Jai Radhe Sales, INDIA	10.03 ± 0.76	5.26 ± 0.08	1365	36.40

force between primary host particles is reduced. Such a shift from Guest-Host to Guest-Guest contact regime occurs at an approximate SAC of 30% as per the model.

The asperity size (d) is typically approximated to be 200 nm for all powders, based on experimental work by Massimalla and Donsi [53]. However, as will be discussed in the results, this assumption is not valid for the majority of pharmaceutical powders that are usually either much smoother or significantly rougher than the ideal 200 nm rough particles [41]. In cases where dry coating with nano-silica guest particles is performed, Eqs. 3 and 4 may be used to compute the amount of SAC based on the weight of the guest used, and in that case, the asperity size (d) is the size of the silica. The minimum separation distance (z_0) is usually taken as 0.4 nm.

It is important to state the assumptions used for calculations in Eqs. 1–5: [1] Spherical mono-disperse host and guest particles, [2] neither host nor guest particles undergo deformation, [3] the guest particles are uniformly coated, of single layer up to SAC of 100%, and are not agglomerated, [4] host surfaces have uniform surface energy, and [5] van der Waals forces are predominant for dry powders, hence electrostatic and capillary forces could be ignored. Under these assumptions, the model could be used to estimate Bo_g of a powder as a dimensionless bulk-scale cohesion force descriptor, requiring key particle-scale inputs: particle size (D), asperity size (d), host and guest (true) density (ρ_p *and* ρ_d), and dispersive surface energy (γ_d) of both host and guest particles.

Materials and Methods

Materials

A total of 19 different powders were used for experiments, including 7 APIs and 12 excipients. The manufacturers, median particle sizes (d_{50}), Sauter mean diameters ($d_{3,2}$), particle (true) densities (ρ_p), and dispersive surface energies (γ_d) of the APIs are presented in Table II, and excipients in Table III, which also mentions material type. For dry coating purposes, two types of nano-silica were used.

Table III Manufacturers, material tTypes, Median Particle Sizes (d_{50}), Sauter Mean Diameters ($d_{3,2}$), Particle (True) Densities (ρ_p), and Dispersive Surface Energies (γ_d) of the Excipients used in this study

Material	Manufacturer	Type	d_{50} (μm)	$d_{3,2}$ (μm)	ρ_p (kg/m^3)	γ_d (J/m^2)
Cornstarch (CS)	Argo	Starch	14.37 ± 0.12	9.40 ± 0.24	1444	32.34
Granulac 200 (Gran200)	Mutchler, Inc., USA	Lactose	27.94 ± 0.80	10.27 ± 0.12	1528	34.37
Granulac 230 (Gran230)			21.98 ± 0.60	7.36 ± 0.18	1546	34.37
Lactose 120 (Lac120)			93.87 ± 1.2	38.93 ± 0.45	1504	37.46
Sorbolac 400 (Sorb400)			8.69 ± 0.44	4.29 ± 0.06	1520	43.44
Pharmatose 350 (Pharm350)	DFE Pharma, USA		28.25 ± 0.94	26.00 ± 0.12	1540	41.82
Pharmatose 450 (Pharm450)			19.19 ± 0.65	17.00 ± 0.14	1543	44.69
Pharmatose DCL11 (DCL11)			115.37 ± 6.12	85.18 ± 4.66	1543	39.48
Avicel 101 (Av101)	FMC Biopolymer, USA	Microcrystall-ine Cellulose (MCC)	64.24 ± 1.12	42.94 ± 0.34	1562	42.33
Avicel 102 (Av102)			116.59 ± 1.46	65.97 ± 0.37	1563	56.05
Avicel 105 (Av105)			18.97 ± 0.52	10.84 ± 0.21	1559	47.80
Avicel 200 (Av200)			185.89 ± 2.77	100.43 ± 0.88	1562	47.11

Hydrophobic Aerosil R972P nano-silica has a nominal particle size of 20 nm [35], particle (true) density of 2650 kg/m^3 [35], and dispersive surface energy of 36.40 mJ/m^2 [48]. Hydrophilic Aerosil A200 nano-silica has a nominal particle size of 12 nm [48], particle (true) density of 2450 kg/m^3 [45], and dispersive surface energy of 42.80 mJ/m^2 [48]. Evonik, USA, donated both nano-silicas.

Surface Modification: Dry Coating Via LabRAM

Dry coating of pharmaceutical powders was carried out in a high-intensity vibrational mixer (LabRAM, Resodyn Corporation, USA). The pharmaceutical powder (50 g) and a certain amount of the nano fumed silica (R972P or A200) was added in a cylindrical plastic jar (8 cm inner diameter, 9.5 cm height, maintaining ~30% fill level by volume) before clamped into the LabRAM. The placed jar was shaken for 5 minutes at 75 G's acceleration with 60 Hz. The amount of nano fumed silica used for each case is based on theoretical surface area coverage (SAC) calculated using Eqs. 3 and 4 [22], and values for each material for 100%SAC are reported in Supplementary Material S1. Details of LabRAM operation may be found elsewhere [48, 54].

Primary Particle Size Distribution (PSD) Analysis

A Rodos/Helos dry dispersion laser diffraction particle sizer (Sympatec, USA) was used to measure primary particle size distribution at the dispersion pressure of 0.5 bar. The dispersion pressure was determined based on dispersion pressure titration that resulted in no appreciable size differences in the range 0.1 to 1 bar as per previous reports [2, 55]. Although entire PSDs were measured using this technique, the data are not reported for brevity; median particle size (d_{50}) and Sauter mean diameter ($d_{3,2}$) statistics for the average of three experimental runs are listed in Tables II and III. The Fraunhofer Enhanced Evaluation (FrEE) and Mie Extended Evaluation (MiEE) theories of light scattering were used to determine particle size by the Helos unit. Experiments were done in triplicates, with average values being reported.

Particle (True) Density Analysis

Each powder's particle (true) density was analyzed via Pycnometer (NOVA 3200, Quantachrome Instruments, Boynton Beach, FL, USA) with Helium gas. Experiments were done five times for each powder, with average values being reported in Tables II and III.

Surface Energy Analysis

An automated inverse gas chromatograph (SEA-iGC, Surface Measurement Systems Ltd., Middlesex, UK) was used to evaluate dispersive surface energy of powders and the results are shown in Tables II and III. About 200–400 mg of powder sample loosely packed into silanized glass columns (4 mm inner diameter, 30 cm length) using a column tapper until no visible channels were seen in the powder bed, bookended with silanized glass wool. Helium, the carrier gas, was used to condition the powders and remove impurities and moisture at a 10 mL/min flow rate for 120 minutes. During the conditioning step, column and injector/detector temperatures were maintained at 30°C and 180°C, respectively. Gas probes (Hexane, Heptane, Octane, Nonane, and Decane) were carried into the column by helium with a flow rate of 10 sccm (standard cubic centimeter per minute). The retention time was detected by an FID and recorded. Lifshitz-van der Waals (LW) dispersive surface energy was attained via the Schultz method [7, 55], and all reported data are for infinite dilution (3% Surface coverage of sample with gas probes). Duplicate measurements were done to ensure reproducibility.

Particle Morphology Analysis: Scanning Electron Microscopy

A particle surface morphology was done using a Field Emission Scanning Electron Microscope (SEM, JSM 7900F, Jeol Ltd., Peabody, MA, USA). Prior to SEM imaging, samples were sputter-coated with Carbon (Q150T, Quorum Technologies Ltd., Laughton, East Sussex, England) to enhance conductivity.

Particle Specific Surface Area Analysis

The specific surface area (SSA) of powders was measured via Brunauer-Emmett-Teller (BET) theory using a Quantachrome ASiQWin, with Autosorb iQ software for analysis. A few grams of powder sample was poured into a 6 mm ID tube with a glass bulb at the bottom. Degassing was carried out under vacuum for 12 hours at 90 C. Afterwards, an 11-point BET adsorption analysis ($P/P_0 = 0.05–0.3$) was conducted using Nitrogen gas at 77 K. SSA values were calculated from adsorption isotherms which have linear R^2 values above 0.9975 and positive C constants. Duplicate measurements were done to ensure reproducibility.

Dynamic Imaging Based Particle Shape Analysis

Particle shape analysis of all materials was conducted using a QicPic/Rodos (Sympatec, USA), which uses high-speed dynamic image analysis to analyze singular particles Field [48, 55, 56] optically. Measurements were done in triplicates, and 0.5 bar dispersion pressure was applied to disperse particles adequately. About 2 g of the powder samples were put on the VIBRI (Sympatec, USA)

vibrating chute. When the measurement starts, the chute vibrates and dispenses the powder into the system. At this point, the Rodos system applies compressed air, providing pressure to disperse the powder into primary particles, while the QicPic system captures 2D images of powder in real time. The image data is then converted into shape and PSD data. For the sake of brevity, only aspect ratio (ratio of largest to smallest dimension) and sphericity (ratio of perimeter to smallest dimension) are analyzed. The details of data analysis may be found elsewhere [56–58]. Experiments were done in triplicates, and average values were reported.

Powder Bulk Properties Evaluation: Shear Test

An FT4 Powder Rheometer (Freeman Technologies, UK) was used to perform shear tests to quantify powder flow via flow function coefficient (FFC, the ratio between the major principal stress and unconfined yield strength) values. The program "Shear_3kPa" was utilized with an acrylic cylinder with dimensions of 25 mm diameter and 10 mm height (25 mL in volume). First, the powder sample was conditioned with a twisted blade and then pre-consolidated at 3 kPa using the vented piston, then splitting and removing the excess powder to create a flat surface. Next, the powder was sheared till failure at 2, 1.75, 1.5, 1.25, and 1 kPa normal stresses using the FT4's shear cell, and incipient failure shear stresses were recorded at each normal stress. Finally, the FT4 Data Analysis v4 software was used to calculate the FFC from the experimental data. The physical interpretations of numerical FFC values are summarized in Table I in Section 1, based on a previous study [25]. The shear tests are done in triplicates, with average values being reported. Further details of the shear test can be found in literature published by Freeman Technologies [59]. One last detail to note is that all FFC results are capped at 32 for Figs. 2 and 7, as values larger than 32 do not have any physical difference, according to Table I. Capping FFC values at 32 allows for a better interpretation of data by providing better visuals of lower FFC values in plots. Including data points above 32 minimizes the visibility of lower FFC values and thus makes for a more difficult interpretation. It is important to note that FFC values are not linearly proportionate to flow classification or categories, which could also be considered as flow regimes analogous to "plastic flow", "inertial flow", "fluidization," and "suspension" depending on the cohesion [23]. For example, an increase from FFC of 1.5 to 2.5 improves the classification from "very cohesive" to "cohesive," according to Table I. However, a powder is still classified as "free-flowing" if FFC values are 15 or 50. Therefore, all FFC values larger than 32 will be reported and plotted at 32. However, for accessing the predictability of flow via Bo_g, FFC values were not capped for better visualization corresponding to power law relation.

Results and Discussion

Scanning Electron Microscopy Images

Pharmaceutical powders exhibit considerable variations in particle morphology, which can influence the bulk powder flow [9]. Therefore, it is crucial to account for particle morphology when investigating powder flow prediction models based on Bo_g, which utilizes particle-scale inputs. Distinct particle morphologies are evident in Fig. 1, which displays SEM images, including spherical (Cornstarch in Fig. 1e), cubic (Ascorbic Acid in Fig. 1b), rough-surfaced (GF in Fig. 1c), rough-surfaced (Sorbolac400 in Fig. 1f), and micronized/cohesive (mAPAP in Fig. 1a). Some materials even display a combination of different particle morphologies, including irregular shape, a higher aspect ratio, and rough surface (e.g., Avicel 102 in Fig. 1g). Additionally, the particle sizes of the materials in the data set vary greatly, from approximately 5 µm to 200 µm, see Tables II and III. Incorporating powders with diverse particle sizes and shapes provides a more inclusive data set, allowing for the derivation of more generalizable conclusions while also identifying which particle-scale characteristics could lead to appreciable deviations from the main trends. Such broadly applicable insights are of greater value to pharmaceutical formulators, which could not be derived from narrower data sets, as discussed in Section 4.4 through examples in Table IV [26, 52].

Effect of Surface Area Coverage on Flow Improvement

Figure 2 displays experimental FFC results plotted against SAC values of 0%, representing no dry coating, 25%, 50%, and 100%. Figure 2a and b are for APIs dry coated with hydrophobic R972P and hydrophilic A200 nano-silica, respectively, and Fig. 2c and d are for excipients dry coated with hydrophobic R972P and hydrophilic A200 nano-silica respectively.

Remarkably, as seen in Fig. 2, flow enhancement is achieved in all cases of dry coated particles, irrespective of the SAC level, host material, or guest material, except for one case of a macro rough powder (GF with A200 50%SAC). For API materials, see Fig. 2a and b, it appears that SAC of 50% is adequate, with marginal flow improvement at higher SAC levels. Interestingly, a higher SAC of 100% led to further FFC increase in a few cases, but

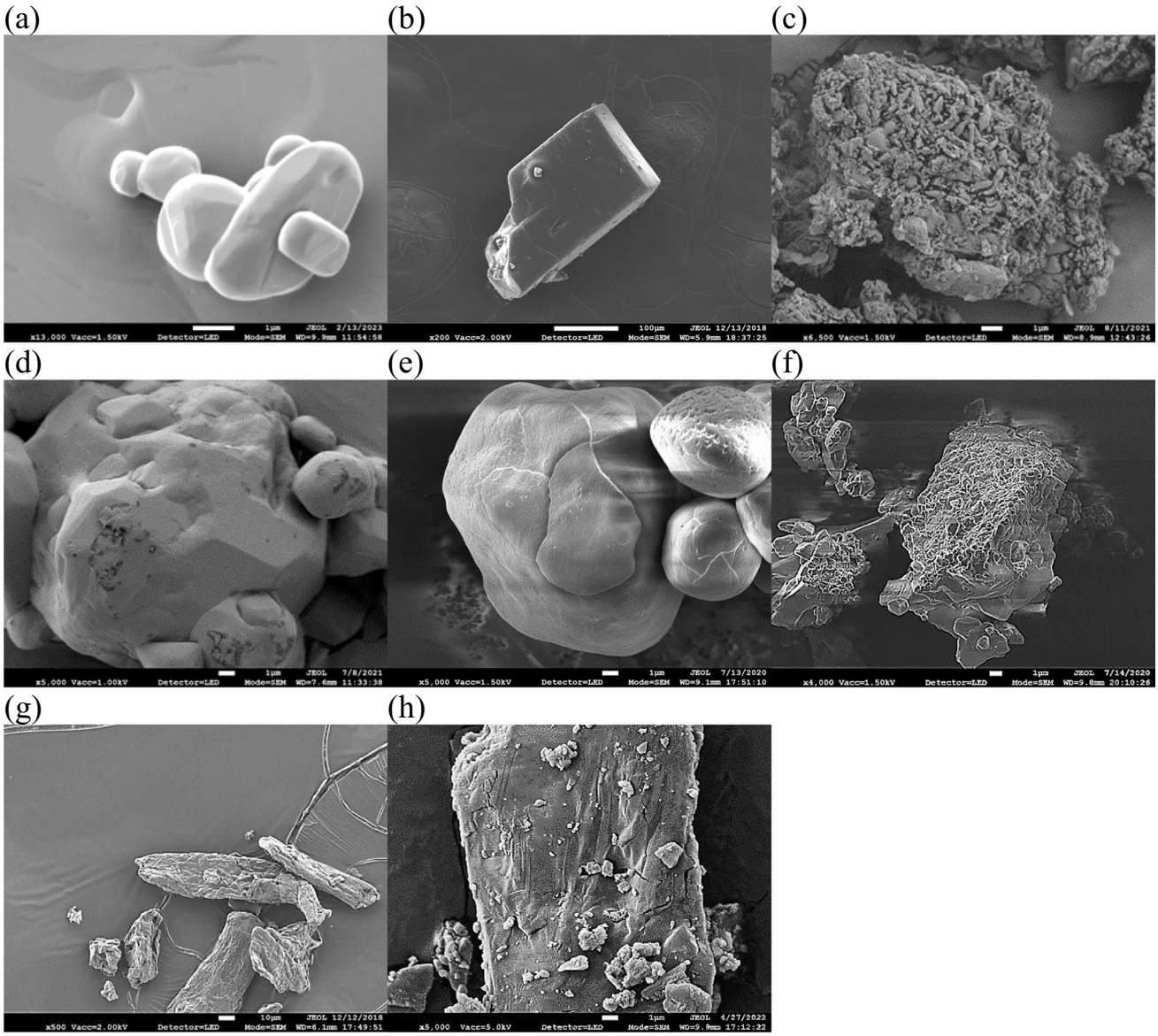

Fig. 1 Scanning electron microscope (SEM) images of various pharmaceutical powders used in this study, including (**a**) micronized Acetaminophen (mAPAP), (**b**) Ascorbic Acid (AA), (**c**) Griseofulvin (GF), (**d**) Fenofibrate (FNB), (**e**) Cornstarch (CS), (**f**) Sorbolac 400 (Sorb400), (**g**) Avicel 102 (Av102), and (**h**) Pharmatose450 (Pharm450)

those powders were already either free-flowing or easy flowing at 50% SAC. For uncoated API powders having FFC values below 4, their FFC values gradually increased as SAC was increased from 25% to 50% SAC, and mostly remained the same between 50% SAC and 100% SAC. For such cohesive API powders with FFC values below 4, these results indicate that 50% SAC of either silica may be adequate and the right choice. For excipients, see Fig. 2c and d, having a wider range of flow categories for uncoated powders, all but three cases achieved easy-flow or free-flow even at 25% SAC, hence there was no advantage of having SAC higher than 50%. In summary, it may be surmised that 50% SAC with either silica may provide the best possible flowability enhancements. These experimental results validate previously published theoretical and simulation models that assured the prevalence of guest-guest contacts at SAC of about 30%, which would provide the best possible flowability enhancements [22, 42].

The experimental results supported by the model confirm that the amount of silica is best determined through normalization based on the surface area coverage (SAC). In contrast, pharmaceutical formulators typically employ weight percentage (wt%) for the flow additive amount, usually 1 wt% in a pharmaceutical blend. As a reference, the wt% of nanosilica used in dry coating, corresponding to various silica %

Table IV Selected Cases of Powder Materials Along with their Size and Surface Descriptions

Material	Nature of Particle Size distribution	Span	Surface roughness	Spacing between the asperities	SSA (m^2/g)
mAPAP*	Broad	3	Smooth Surfaced	N.A.	0.77
FNB	Narrow	1.81	Smooth Surfaced	N.A.	0.94
GF	Broad	2.03	Rough Surfaced	Same order as asperities	5.03
Sorb400	Very Broad	4.29	Rough Surfaced	Same order as asperities	2.62
Corn-Starch	Unimodal	1.03	Smooth surfaced	N.A.	0.33
Pharm450	Broad	2.34	Presence of fines on surface	Uneven/sparse	2.20
Av105*	Narrow	1.96	Rough Surfaced	Uneven/ Sparse	1.57
Av101*	Narrow	1.90	Rough Surfaced	Uneven/ Sparse	1.49
Av102*	Narrow	1.15	Rough Surfaced	Uneven/ Sparse	0.91
Av200*	Narrow	1.45	Rough Surfaced	Uneven/ Sparse	1.05

**Represents powder materials common with Capece et al.* [61]

SAC, is provided in Supplementary Material S1. The wt% data is also plotted in Fig. 3 for the sake of benchmarking against % SAC for very cohesive and cohesive (FFC < 4) APIs and excipients that usually require larger wt%. APIs dry coated with hydrophobic R972P and hydrophilic A200 in Fig. 3a and b, respectively, and excipients dry coated with hydrophobic R972P and hydrophilic A200 in Fig. 3c and d, respectively. The connecting lines depict the same material at varying SAC levels. It is seen from Fig. 3 that unlike % SAC, the ideal nano-silica wt% achieving the best level of flow improvement varies widely. Fortunately, 1 wt% (vertical dashed line in each plot) silica may be adequate for most powders, except for a few APIs (Fig. 3a). The claim concerning 50%SAC is reaffirmed, as it becomes evident that most powders do not demonstrate considerable improvement beyond this threshold. Notably, this level also corresponds to under 1 wt% silica content for most of the powders, a fact visually marked by star-shaped red colored markers, denoting the 50%SAC scenario. That means the amount of silica greater than 1 wt% is seldom necessary. In summary, the results depicted in Figs. 2 and 3 highlight the benefit of relying on the normalized silica amounts in the form of theoretical SAC instead of relying on silica wt%.

Effect of Nano-Silica Guest Type on Flow Improvement

It is generally believed that R972P nano-silica is better than similar hydrophilic silica for flow enhancement due to its hydrophobic nature, which facilitates easier nano-silica deagglomeration and dispersion over the host particle's surface [35, 43, 47, 60]. Conversely, the hydrophilic nature of A200 nano-silica is expected to be less effective in deagglomeration and spreading. Here, the relative performance of either silica type is assessed experimentally. It is noted that if the dry coating process were to be equally effective for either silica, and there was no difference in the surface energy of APIs after either silica coating, Eq. 5 might suggest that A200 could perform better due to its smaller size. However, the specific dispersive surface energy of A200 [41, 60] is higher than that of R972P. Detailed analysis of the contact model (Eq. 5), while outside the scope for the current paper, requires careful consideration of two terms representing adhesion after dry coating; [1] a non-contact term (between two original host particles, separated by an asperity), and, [2] a contact term that is between the asperity and a contacting host (or another asperity on the contact host). As the asperity size increases, the non-contact term decreases. However, as asperity size increases, the contact term increases. Thus the total leads to an "optimal" asperity size which is a complex function of the host size, asperity size, and surface energies. Hence, when considering the coating effectiveness differences between hydrophobic and hydrophilic silicas, predicting which would perform better for which hosts is very difficult, if not impossible based on the currently available models.

Experimental results for three different % SAC values are plotted against uncoated FFC values in Fig. 4. Two lines are individually fitted to the data, each corresponding to the best-fit line for A200 and R972P silica cases. Visually, there are points representing both A200 and R972P coatings at each SAC level that are closely situated, suggesting some powders exhibit slightly better results with A200 and some others with R972P. Nonetheless, R972P slightly outperforms A200 in most cases, more so for SAC values of 50% and 100%. A few cases of interest are noted based on the FFC values of about 2, 3, and 4 for uncoated APIs. These are Itraconazole, GF, and IBU50, respectively. At 25% SAC, R972P outperforms A200 in terms of FFC of dry coated Itraconazole and GF, although A200 performed better for IBU50. However, at higher SAC values, R972P considerably outperforms A200, such that all three R972P coated APIs

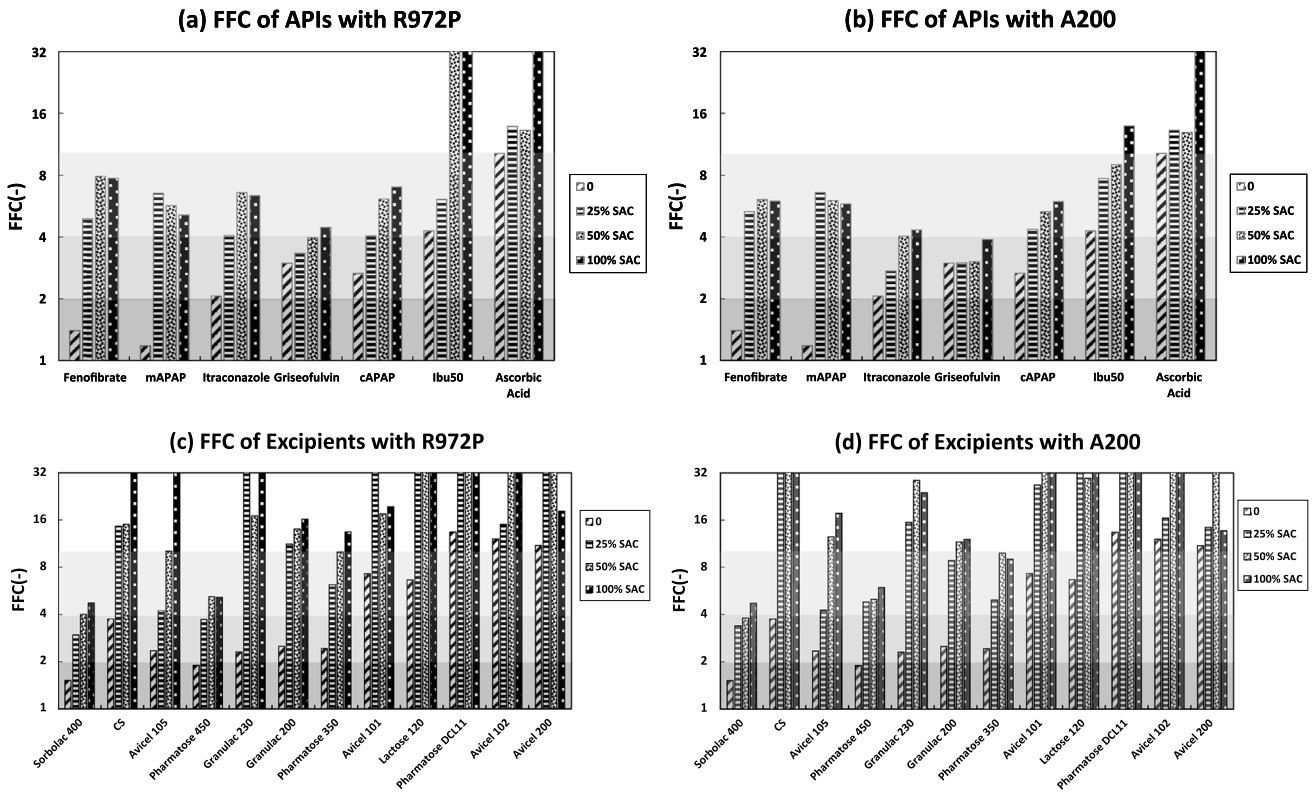

Fig. 2 Flow function coefficient (FFC) as a function of surface area coverage (SAC) of (**a**) host active pharmaceutical ingredients (APIs) by hydrophobic R972P nano-silica, (**b**) host APIs by hydrophilic A200 nano-silica, (**c**) host excipients by R972P, and (**d**) host excipient by A200

are almost one flow category better, and there is an appreciable advantage of using R972P as the guest particle over A200. Regardless, the average trend lines for R972P and A200 in these three plots in Fig. 4 indicate a lack of striking difference between the two types of silica. In general, such results convey that the level of enhancements from either silica may be similar, although they are the overall result of the coating effectiveness in addition to their size and specific dispersive energy values.

Next, the relative performance of the nano-silicas is examined through the number of powders that are free-flowing (FFC > 10) after dry coating at various SAC levels, see Fig. 5. That is because, in the end, making the powder, in particular the API, free-flowing would be the most desirable outcome. The dashed line in Fig. 5 represents the fraction (0.21) of powders that are already free-flowing prior to dry coating. Here too, the number of free-flowing powders after dry coating with R972P (black bars) are higher than those coated with A200 (gray bars), albeit by only one or two powders at each SAC level. Figure 5 confirms the observation from Fig. 4 and the consensus that hydrophobic R972P is better for flow improvement, although only marginally.

While achieving free-flow category is desirable, it is useful to know how these silicas perform for very cohesive powders based on the flow classes of the uncoated particles. As previously noted, an increase in FFC by even one unit is significant for very cohesive powders. For example, if the FFC of a powder improves from 1.5 (very cohesive) to 2.5 (cohesive), it has been enhanced by one flow category. But an increase from 1.5 (very cohesive) to 4.5 (easy flowing) means two flow category improvements, which is rather substantial. The extent of such enhancements is examined in Fig. 6, which presents the number of flow category improvements among different initial flow categories at each SAC level. As an example, the first bar in Fig. 6a, belonging to the "very cohesive" flow class, shows a total of 4 powders within that category; 3 of them exhibit two category improvements, and one demonstrates a single category improvement at 25%SAC, and so on for other levels of SAC. Overall, only minor differences between each nano-silica type can be observed, although generally, R972P slightly outperforms A200.

In summary, Figs. 4, 5 and 6 indicate slight differences between hydrophobic R972P and hydrophilic A200 nano-silicas at various SAC levels, although R972P performs marginally better at enhancing flowability. As a positive message, the formulators who prefer to stay with hydrophilic

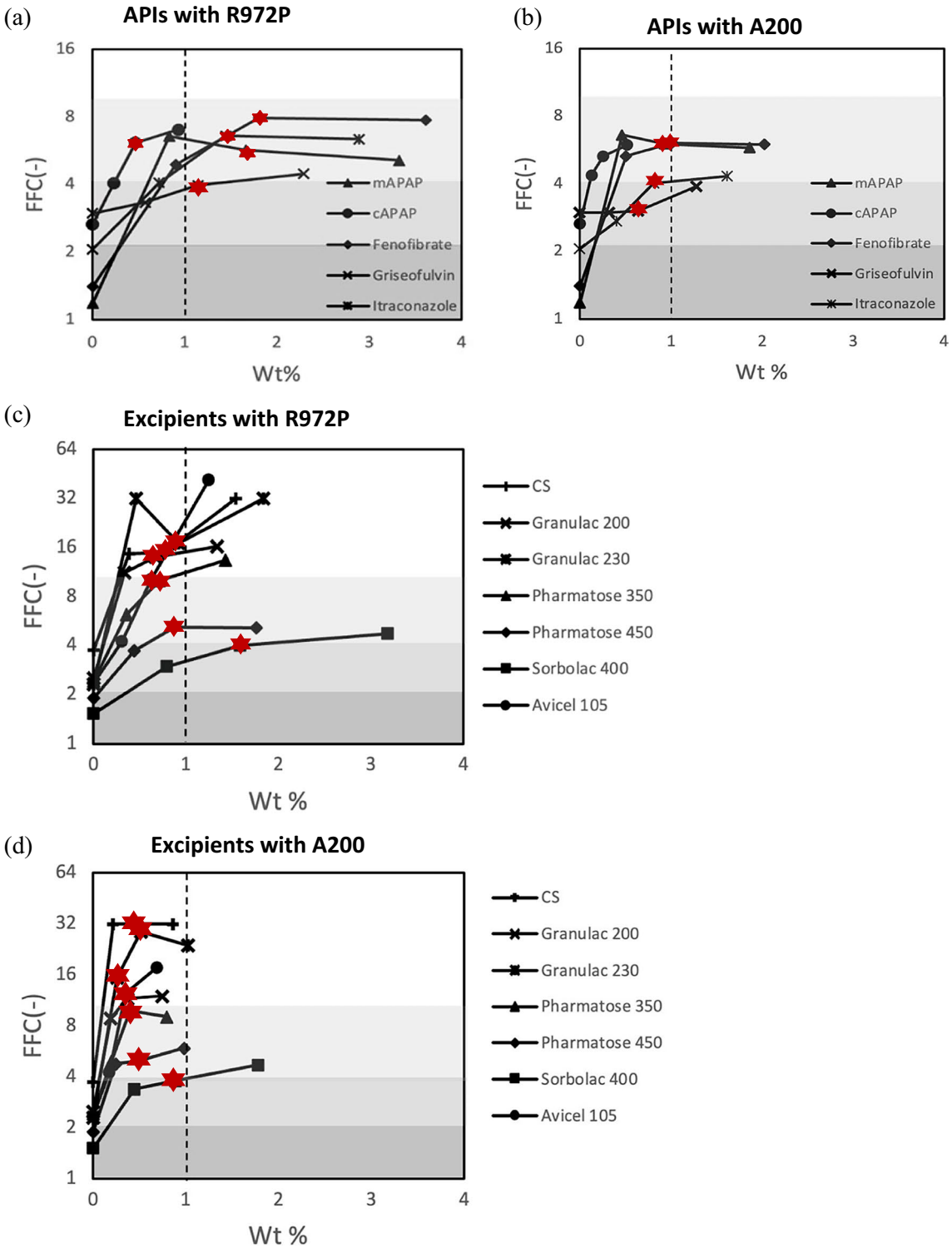

Fig. 3 Flow function coefficient (FFC) plotted against weight percentage of guests for (**a**) host active pharmaceutical ingredients (APIs) with hydrophobic R972P nano-silica, (**b**) host active pharmaceutical ingredients (APIs) with hydrophobic A200 nano-silica, (**c**) host excipients with hydrophobic R972P and (**d**) host excipient with hydrophobic A200 nano-silica. Only cohesive or very cohesive (FFC < 4) APIs and excipients are plotted; 50%SAC cases are highlighted using red stars, denoting that in most cases, 1 wt% silica is adequate

silica for various reasons, including but not limited to the API being poorly water-soluble, need to take comfort from the results presented that A200 is an excellent alternative to using hydrophobic silica. It should be noted that although A200 performs rather well, different hydrophilic silica, e.g., M5P (Cabot Inc., USA), may not perform as well

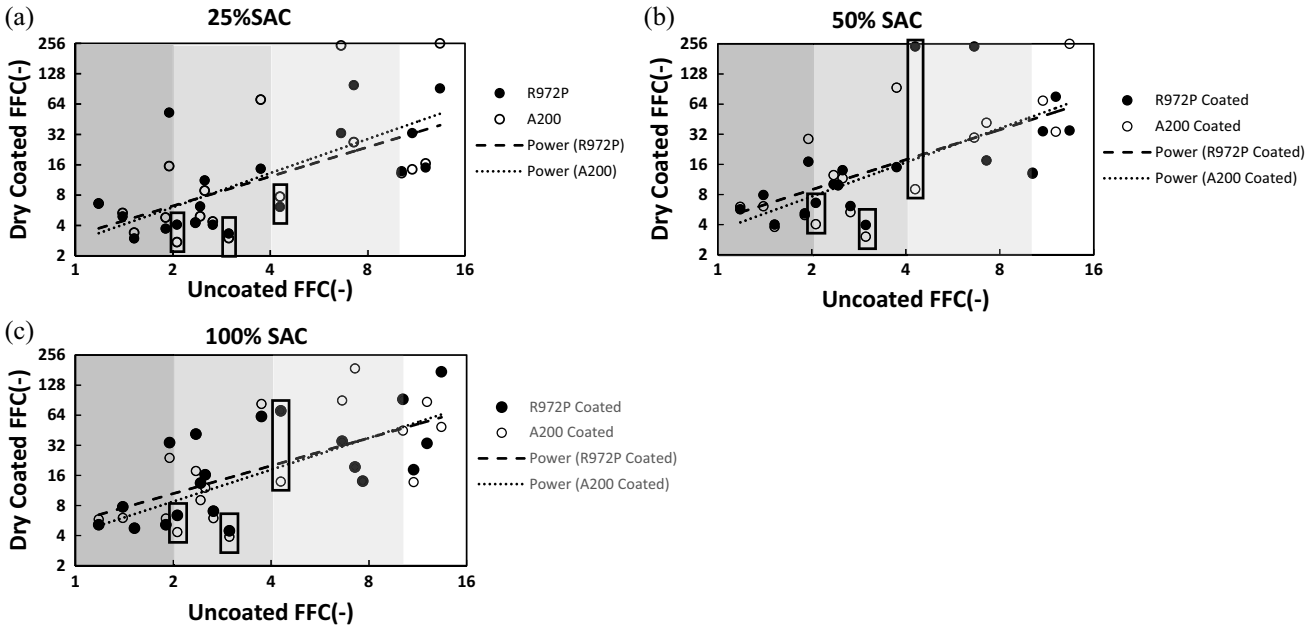

Fig. 4 FFC values for dry-coated powders (y-axis) are plotted against that of uncoated powders (x-axis) for all powders of Fig. 2 at (**a**) 25% surface area coverage (SAC), (**b**) 50% SAC and (**c**) 100% SAC for each silica type

because it has a size comparable to R972P (20 nm) and has higher specific surface energy as compared to A200 [35, 36, 43–45, 51]. A closer examination of different hydrophilic silicas is outside the scope of this paper and will be reported in a future paper.

Assessing Predictability of Powder Flow from Particle-Scale: Nondimensionalization through Bond Number

Predicting powder flow from particle-scale properties is desirable but rather difficult since powder flowability is a bulk-behavior that would also depend on the ensemble behavior rather than just individual particle properties [21, 27, 54]. Clearly, predicting flowability based on particle size alone is not possible for the particles that are dry coated or otherwise surface modified since the particle size or the size distribution are not appreciably changed due to dry coating. In contrast, the flowability is dramatically different, as evident from the results presented so far. Nonetheless, the possibility for prediction based on size alone is examined next. Figure 7 presents the FFC values plotted against the median particle size (d_{50}, Fig. 7a) and Sauter mean diameter (d_{32}, Fig. 7b) for both uncoated and 100% SAC R972P dry-coated powders. Only R972P coated powders at 100% SAC representing the ideal performance are shown for brevity. The open markers represent experimental data for uncoated powders, whereas the solid markers denote experimental data for powders dry coated with R972P nano-silica. The dashed line is the best-fit power-law line for uncoated powders, for which the FFC values are reasonably correlated with particle size. However, for dry coated powders, the FFC values are much higher, while the particle size remained the same in both plots. An approximate trend line passing through all dry coated points is drawn for each plot. The visual separation between these lines and the best-fit power-law lines for uncoated powders convey that as expected, particle size cannot be the sole input in a flow prediction model.

Next, Bo_g as a dimensionless ratio of interparticle attractive forces and the weight of the particle is considered as the basis for flowability prediction. The computation of Bo_g requires four particle-level factors: particle size (D), actual particle density (ρ_p), asperity scale (d), and dispersive surface energy (γ_d). However, the powder sample consists of diverse morphologies and particle size distributions, and the choice of which size to pick is not apparent. For the sake of simplicity, d_{32} values were used for calculating Bo_g [61]. With regard to the asperity scale for all powders, both a smooth surface assumption and a "200 nm" inherent roughness assumption were considered. Figure 8a presents the experimental FFC values of all API powders plotted against Bo_g numbers for both uncoated and dry coated APIs; open circles represent Bo_g estimated assuming the natural roughness of 200 nm, and open squares are for Bo_g estimated assuming the naturally smooth powders. All dry coated APIs with 100% SAC R972P are shown as solid circles. Particles with $Bo_g < 0.01$ were excluded, being cohesionless and free-flowing. For each case of as-received API natural surface roughness assumption, power-law trends are shown. The solid line represents the smooth surface assumption,

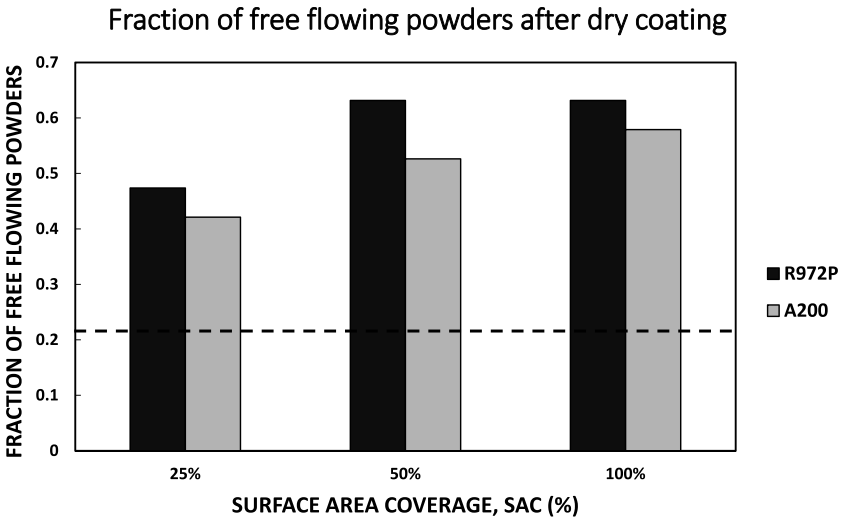

Fig. 5 Fraction of the total number of free-flowing powders (FFC > 10) at each surface area coverage (SAC) level. The horizontal dashed line represents the fraction of the total number of free-flowing powders before dry coating

and the dashed line represents the 200 nm rough surface assumption. Since Bo_g for dry coated API powders could be estimated using the asperity size to be the same as silica size, only a single set of points need to be plotted. These trend lines indicate that for this set of API powders, both the uncoated and dry coated outcomes are better captured under the smooth surface approximation. That suggests that the 200 nm roughness assumption proposed for fluidized-bed cracking catalyst (FCC) powders [53] is not applicable for crystalline APIs. For both the uncoated and dry coated API powders, there is some scatter around the trend line (solid line). Amongst the uncoated API powders, mAPAP, FNB, and GF, highlighted through arrows in the figure, indicate slight deviations from the trend. Actual FFC for mAPAP and FNB are lower than predicted by the solid best-fit line, whereas the FFC of GF is higher than predicted. It is important to note that Bo_g computed for the fitted solid trend line are based on smooth surface assumption, yet the APIs such as GF are not smooth. Hence, the trend-line could be biased in a manner that may not capture some of the smooth APIs, e.g., mAPAP and FNB. Their lack of roughness is also generally corroborated by their specific surface area value, which is less than 1 m^2/g, see Table IV. In contrast, GF is less cohesive than predicted because it has a notably rough surface, with dense distribution of asperities such that the distance between the neighboring asperities is small, about the same scale as the size of the asperities. Such morphology is also corroborated by its $>>1$ specific surface area value of 5.03 m^2/g (Table IV). For dry coated API powders, most FFC values follow the same trend-line corresponding to the assumption of smooth surfaces of the uncoated powders. It is seen that the FFC enhancement for GF is much lower than predicted and may be attributed to its rough surface and corresponding high SSA, which may reduce the effectiveness of silica coating, not to mention that it may require higher levels of silica. There are also deviations in the actual and predicted FFC values of the dry coated APIs for the cases when FFC > 10. However, such a high FFC value indicates they all belong to the free-flow category; hence, accurate FFC prediction would be unnecessary and meaningless. Overall, using a variety of APIs, of which only mAPAP (marked by "*" in Table IV) is common with a previous paper [26], confirms that Bo_g is a great choice for predicting flowability of both uncoated and dry coated powders.

Figure 8b presents the experimental FFC values of all excipient powders plotted against Bo_g for both uncoated and dry coated powders. The open circles represent Bo_g estimated assuming the natural roughness of 200 nm, and open squares are for Bo_g estimated assuming the naturally smooth powders. All dry coated excipients with 100% SAC R972P are shown as solid circles, and the power-law fitted solid line represents the smooth surface assumption, and the dashed line represents the 200 nm rough surface assumption. As is the case for the APIs, the smooth surface approximation for Bo_g estimation works better. There are no major deviations, although uncoated FFC for Sorbolac400 is slightly higher, whereas dry coated FFC is lower than predicted by the trend-line, both may be explained by its surface roughness and higher SSA values (Table IV), like that for GF. The situation with Pharmatose450, also highlighted in Fig. 8b, is similar yet less pronounced. The rest of the excipients tested, including MCCs (marked by "*" in Table IV) that are common with a previous paper [26], are fitted well through the power-law as seen in Fig. 8b, further confirming that Bo_g is a great choice for predicting flowability of both uncoated and dry coated powders. Finally, as was the case for dry coated APIs, there are deviations in the actual and predicted FFC values of the dry coated excipients for the cases when FFC > 10. However, as mentioned before, such high FFC value indicates they all belong to the free-flow category, and hence accurate FFC prediction would be unnecessary and meaningless. Finally, Fig. 8c and d present a consolidated view

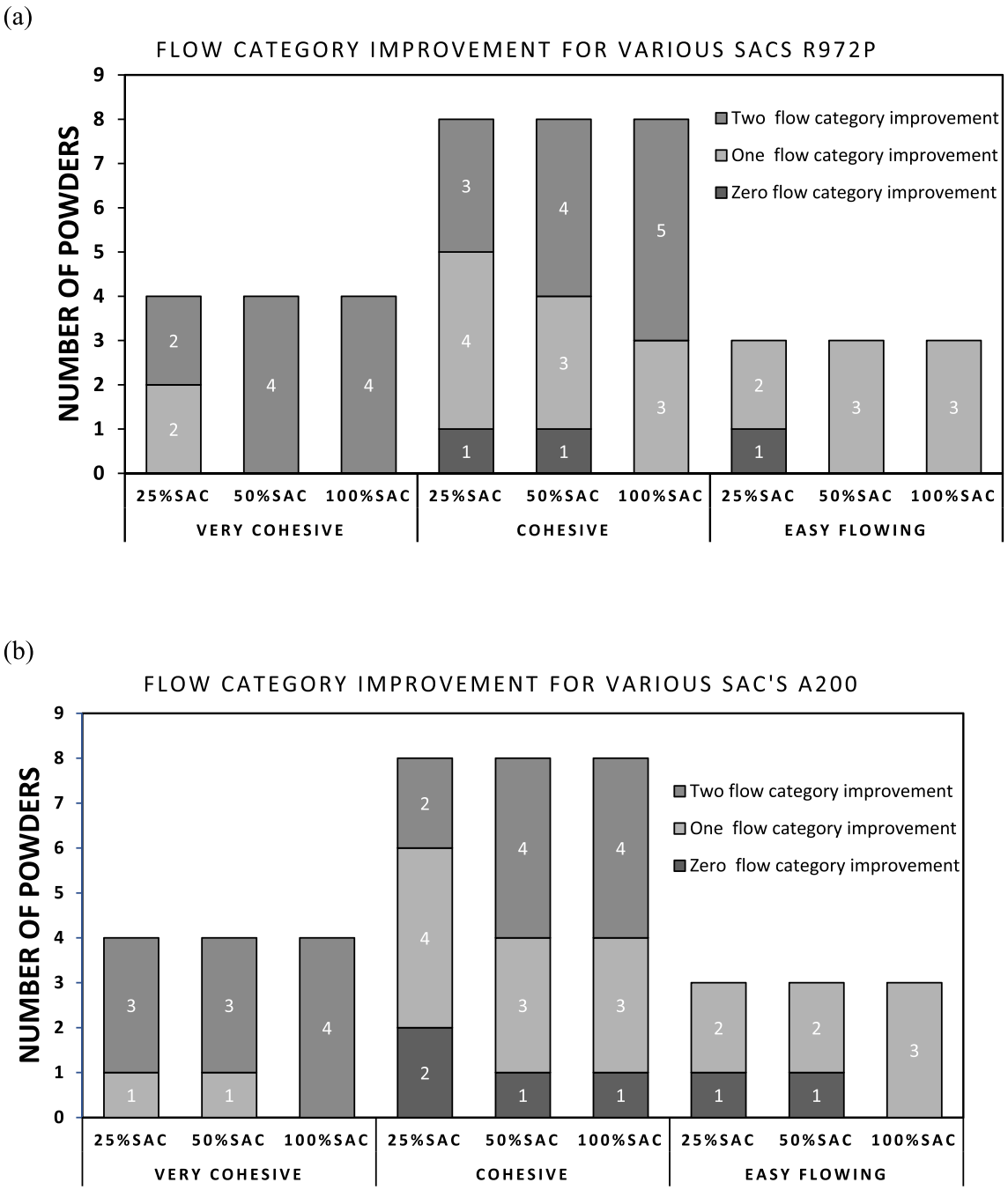

Fig. 6 The number of powders based on flow category improvement from initial flow category (**a**) With A200 coating, (**b**) With R972P nano silica coatings for different SACs (Note: 4 powders that are in free-flowing category before dry coating are not presented)

of trends for both APIs and excipients. Figure 8c depicts the Bo_g calculations premised on the smooth surface approximation, while Fig. 8d employs a consideration of 200 nm surface roughness. Interestingly, combining APIs and excipients together reconfirms a coherent trend where the smooth surface approximation aligns more accurately with the observed data. This coherency is particularly significant given that most of the powders in the current work inherently possess smooth surface characteristics. Therefore, Fig. 8c, which is based on smooth surface prior to dry coating, effectively illustrates a more fitting representation of the trends in the datasets of both APIs and excipients combined together.

In summary, the power-law relation between the FFC and Bo_g is evident from Fig. 8 and predictability is likely to improve if the surface roughness for each powder could be better estimated. The inclusion of a diverse set of API and excipient materials ranging in size, aspect ratio, and surface roughness makes this outcome more generalizable as

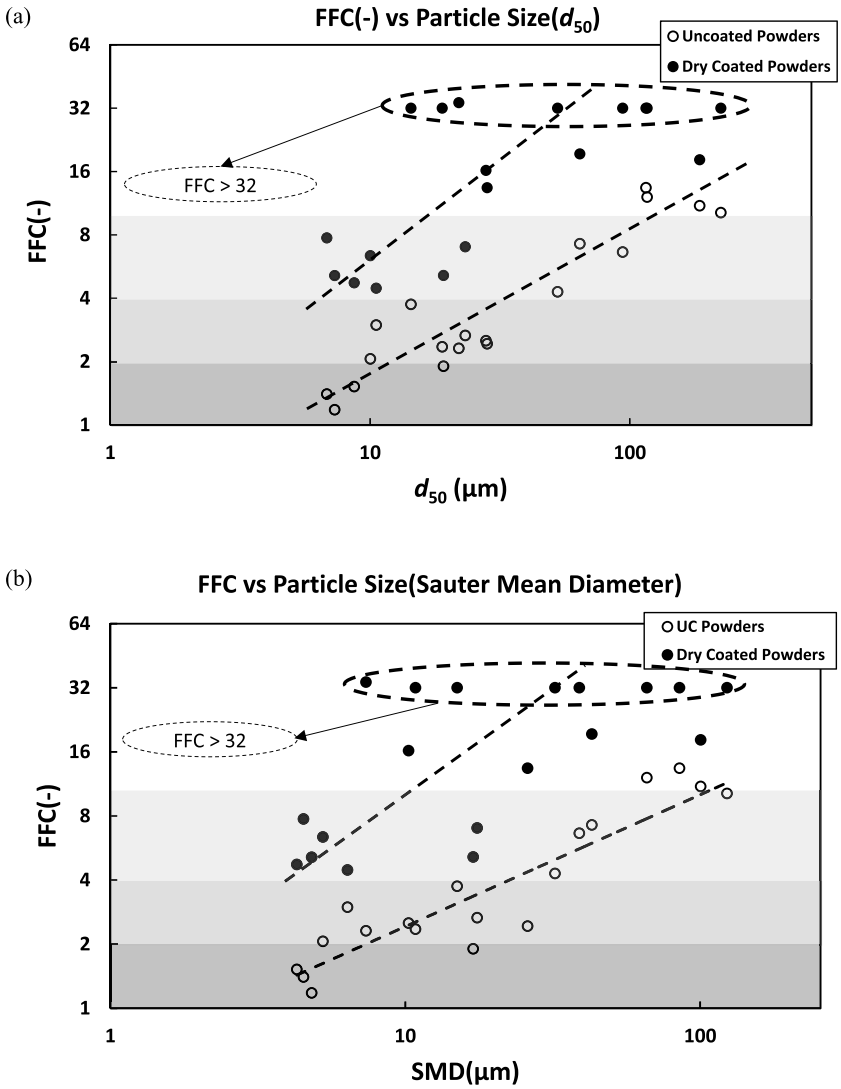

Fig. 7 Flow function coefficient (FFC) plotted against (**a**) median particle size (d 50) and (**b**) Sauter mean diameter (d 32) for uncoated powders (open markers) and powders dry coated (dark markers) with R972P at 100% surface area coverage. The shading in the background corresponds to the flow classification found in Table 1

compared to previously published papers and confirms that silica dry coating is a viable approach for dramatic flowability enhancement.

Conclusions

A comprehensive set of pharmaceutical powders having different sizes, surface roughness, morphology, and aspect ratios provided exemplary test cases to investigate the effect of dry coating the amount and type of silica on powder flowability enhancement. Normalization of silica amount in the form of theoretical surface area coverage (SAC) better helped understand the relative performance as silica amount varied, instead of using fixed wt% amounts. Nearly maximal flow enhancement was observed for all powders at about 50% SAC of either type of silica, hydrophobic R972P, or hydrophilic A200, although R972P generally performed better. This consistency in performance as a function SAC in contrast with wider variability in wt% suggests that SAC is a more reliable parameter for industry practice. Fortunately, the amount of silica required was 1 wt% or much less for a large majority of cases. Dry coating of these powders resulted in one or more category flow enhancements, which were significant in situations where flow improvement would be most beneficial. For example, at 50% SAC with R972P, all uncoated, *very cohesive* powders gained two flow category, attaining the *easy-flow* class. For cohesive powders, flow improved by one or more categories or at least by one or more FFC units. Detailed analysis of the results indicated that the particle size alone could not predict flowability for both the uncoated and dry coated powders. Fortunately, even with the inclusion of a diverse set of powders, the predictive capability was significantly better through non-dimensionalization of cohesion through Bond number based on the mechanistic multi-asperity particle contact model accounting for the particle size, surface energy, roughness, and the amount and type of silica. The power-law relation between

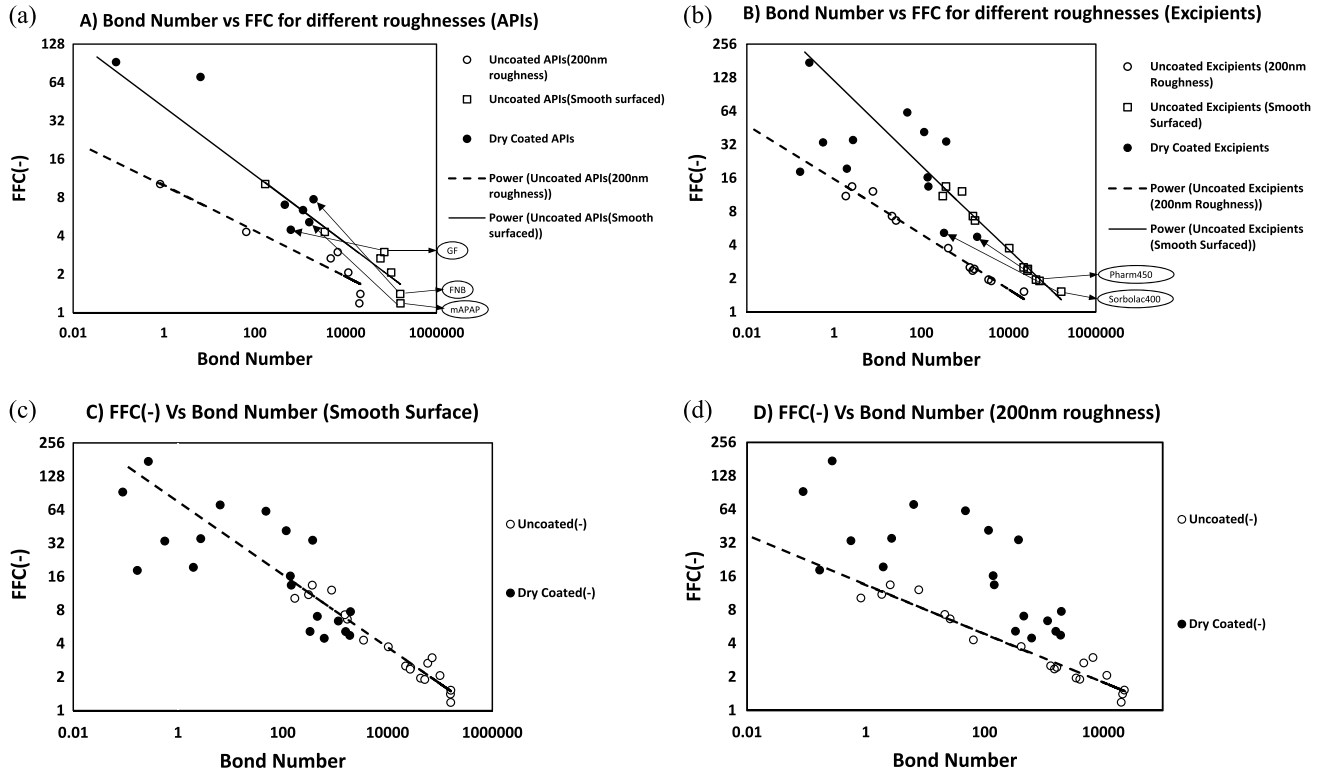

Fig. 8 Flow Function Coefficient for R972P coated powders both before and after dry coating plotted against Bond Number calculated using Sauter mean diameter (d32) and using 200 nm natural roughness as well as a smooth surface approximation for uncoated powders, (**a**) For APIs, (**b**) For excipients, (**c**) combining APIs and excipients with smooth surface approximation, and (**d**) combining APIs and Excipients for 200 nm natural roughness approximation

FFC and Bond number observed here validates previous work that demonstrated such a relationship between particle-scale and bulk-scale properties [7, 21–23, 26, 27, 57]. As a major novelty, it was found that the widely accepted 200 nm surface roughness is not valid for most pharmaceutical powders. Therefore, accurately estimating surface roughness is crucial for more truthful Bond number computation for better capturing powder flow behavior. It is also noted that a high specific surface area (SSA) value is a major indicator of particle surface macro-roughness. In summary, the capability to predict flow behavior and its enhancement through multi-asperity contact models and the Bond number is expected to greatly benefit practitioners who can determine the suitability of dry coating *apriori*, without having to conduct full-scale Design of Experiments.

Supplementary Information The online version contains supplementary material available at https://doi.org/10.1007/s11095-023-03561-6.

Acknowledgments The authors thank Zhixing Lin for his valuable input during the writing of this paper.

Author Contribution Kuriakose T. Kunnath: Conceptualization (equal); Writing – original draft (lead); Methodology; Investigation; Validation; Data Curation; Formal analysis; Visualization.

Siddharth Tripathi: Data Curation; Formal analysis; Visualization; Writing – review & editing.

Sangah S. Kim: Writing – review & editing.

Liang Chen: Supervision (support).

Kai Zheng: Supervision (support).

Rajesh N. Dave: Funding Acquisition (lead); Conceptualization (equal); Writing – review, editing and rewriting (lead); Data curation (equal); Formal Analysis (equal); Supervision (lead).

Funding The authors are thankful for financial support from National Science Foundation under grant IIP-1919037, IIP-2137209. RND gratefully acknowledges International Fine Particle Research Institute's (IFPRI) financial support.

Declarations

Conflict of Interest The authors have no conflicts of interest or sources of competing interest to declare.

References

1. Prescott JK, Garcia TP. A solid dosage and blend content uniformity troubleshooting diagram. Pharm Technol North Am. 2001;25(3):68–88.
2. Jallo LJ, Ghoroi C, Gurumurthy L, Patel U, Davé RN. Improvement of flow and bulk density of pharmaceutical powders using surface modification. Int J Pharm. 2012;423(2):213–25.

3. Ghoroi C, Gurumurthy L, McDaniel DJ, Jallo LJ, Davé RN. Multi-faceted characterization of pharmaceutical powders to discern the influence of surface modification. Powder Technol. 2013;236:63–74.
4. Huang Z, Xiong W, Kunnath K, Bhaumik S, Davé RN. Improving blend content uniformity via dry particle coating of micronized drug powders. Eur J Pharm Sci. 2017;104:344–55.
5. Guerin E, Tchoreloff P, Leclerc B, Anguy TD, Deleuil M, Couarraze G. Rheological characterization of pharmaceutical powders using tap testing, shear cell and mercury porosimeter. Int J Pharm. 1999;189(1):12.
6. Nase ST, Vargas WL, Abatan AA, McCarthy JJ. Discrete characterization tools for cohesive granular material. Powder Technol. 2001;116(2–3):214–223.
7. Jallo LJ, Chen Y, Bowen J, Etzler F, Dave R. Prediction of interparticle adhesion force from surface energy and surface roughness. J Adhes Sci Technol. 2011;25(4–5):367–84.
8. Kunnath K, Chen L, Zheng K, Davé RN. Assessing predictability of packing porosity and bulk density enhancements after dry coating of pharmaceutical powders. Powder Technol. 2021;377:709–22.
9. Podczeck F, Miah Y. The influence of particle size and shape on the angle of internal friction and the flow factor of unlubricated and lubricated powders. Int J Pharm. 1996;144(2):187–94.
10. Jallo LJ, Schoenitz M, Dreizin EL, Dave RN, Johnson CE. The effect of surface modification of aluminum powder on its flowability, combustion and reactivity. Powder Technol. 2010;204(1):63–70.
11. Hou H, Sun CC. Quantifying effects of particulate properties on powder flow properties using a ring shear tester. J Pharm Sci. 2008;97(9):9.
12. Kachrimanis K, Karamyan V, Malamataris S. Artificial neural networks (ANNs) and modeling of powder flow. Int J Pharm. 2003;250(1):13–23.
13. Bertuola D, Volpato S, Canu P, Santomaso AC. Prediction of segregation in funnel and mass flow discharge. Chem Eng Sci. 2016;150:16–25.
14. Polizzi MA, Franchville J, Hilden JL. Assessment and predictive modeling of pharmaceutical powder flow behavior in small-scale hoppers. Powder Technol. 2016;294:30–42.
15. Antikainen OK, Rantanen JT, Yliruusi J. Use of the Kohonen self-organising map to predict the flowability of powders. STP Pharma Sci. 2000;10(5):349–54.
16. Guo A, Beddow JK, Vetter AF. A simple relationship between particle shape effects and density, flow rate and Hausner ratio. Powder Technol. 1985;43(3):279–84.
17. Mullarney MP, Leyva N. Modelling pharmaceutical powder flow performance using particle size distribution. Pharmaceutical Technology. 2009;33:126–34.
18. Sandler N, Wilson D. Prediction of granule packing and flow behavior based on particle size and shape analysis. J Pharm Sci. 2010;99(2):958–68.
19. Wang Y, Snee RD, Meng W, Muzzio FJ. Predicting flow behavior of pharmaceutical blends using shear cell methodology: a quality by design approach. Powder Technol. 2016;294(Supplement C):22–9.
20. Yu W, Muteki K, Zhang L, Kim G. Prediction of bulk powder flow performance using comprehensive particle size and particle shape distributions. J Pharm Sci. 2011;100(1):284–93.
21. Yu AB, Feng CL, Zou RP, Yang RY. On the relationship between porosity and interparticle forces. Powder Technol. 2003;130(1–3):70–6.
22. Chen Y, Yang J, Dave RN, Pfeffer R. Fluidization of coated group C powders. AICHE J. 2008;54(1):104–21.
23. Castellanos A. The relationship between attractive interparticle forces and bulk behaviour in dry and uncharged fine powders. Adv Phys. 2005;54(4):263–376.
24. Chen Y, Jallo L, Quintanilla MAS, Dave RN. Characterization of particle and bulk level cohesion reduction of surface modified fine aluminum powders. Colloids Surf A Physicochem Eng Asp. 2010;361(1–3):14.
25. Schulze D. Powders and bulk solids: behavior, characterization, storage and flow. Berlin Heidelberg: Springer; 2007.
26. Capece M, Ho R, Strong J, Gao P. Prediction of powder flow performance using a multi-component granular bond number. Powder Technol. 2015;286:561–71.
27. Capece M, Huang Z, To D, Aloia M, Muchira C, Davé RN, Yu AB. Prediction of porosity from particle scale interactions: surface modification of fine cohesive powders. Powder Technol. 2014;254:103–13.
28. Yang J, Sliva A, Banerjee A, Dave RN, Pfeffer R. Dry particle coating for improving the flowability of cohesive powders. Powder Technol. 2005;158(1–3):21–33.
29. Vercruysse J, Delaet U, Van Assche I, Cappuyns P, Arata F, Caporicci G, De Beer T, Remon JP, Vervaet C. Stability and repeatability of a continuous twin screw granulation and drying system. Eur J Pharm Biopharm. 2013;85(3):7.
30. Van Snick B, Holman J, Vanhoorne V, Kumar A, De Beer T, Remon JP, Vervaet C. Development of a continuous direct compression platrom for low-dose drug products. Int J Pharm. 2017;529(1–2):17.
31. Simonaho S-P, Ketolainen J, Ervasti T, Toiviainen M, Korhonen O. Continuous manufacturing of tablets with PROMIS-line — introduction and case studies from continuous feeding, blending and tableting. Eur J Pharm Sci. 2016;90:38–46.
32. Huang Z, Scicolone JV, Gurumuthy L, Davé RN. Flow and bulk density enhancements of pharmaceutical powders using a conical screen mill: a continuous dry coating device. Chem Eng Sci. 2015b;125:209–24.
33. Kim S, Bilgili E, Davé RN. Impact of altered hydrophobicity and reduced agglomeration on dissolution of micronized poorly water-soluble drug powders after dry coating. International Journal of Pharmaceutics. 2021;606.
34. Chen H, Aburub A, Sun CC. Direct compression tablet containing 99% active ingredient—a tale of spherical crystallization. J Pharm Sci. 2019;108(4):1396–400.
35. Huang Z, Scicolone JV, Han X, Davé RN. Improved blend and tablet properties of fine pharmaceutical powders via dry particle coating. Int J Pharm. 2015a;478(2):447–55.
36. Kunnath K, Huang Z, Chen L, Zheng K, Davé R. Improved properties of fine active pharmaceutical ingredient powder blends and tablets at high drug loading via dry particle coating. Int J Pharm. 2018;543(1–2):288–99.
37. Mullarney MP, Beach LE, Davé RN, Langdon BA, Polizzi M, Blackwood DO. Applying dry powder coatings to pharmaceutical powders using a comil for improving powder flow and bulk density. Powder Technol. 2011a;212(3):397–402.
38. Han X, Ghoroi C, To D, Chen Y, Davé R. Simultaneous micronization and surface modification for improvement of flow and dissolution of drug particles. Int J Pharm. 2011;415(1–2):185–95.
39. Chen Y, Quintanilla MAS, Yang J, Valverde JM, Dave RN. Pull-off force of coated fine powders under small consolidation. Physical Review E. 2009;79(4):041305.
40. Chen Y, Quintanilla MAS, Yang J, Valverde JM, Dave RN. Pull-off force of coated fine powders under small consolidation. Phys Rev E. 2009;79(4):041305.
41. Kim S. C. Cheikhali, Dave RN. Decoding fine API agglomeration as a key indicator of powder flowability and dissolution: impact of particle engineering. Pharm Res. 2022a;20
42. Deng X, Davé RN. Adhesion and friction of dry-coated nano-rough particles. Powder Technol. 2017;314:20–7.

43. Ma B, Jiang Q, Huang J, Wang X, Leng J. Effect of different silica particles on flowability of gypsum powder for 3D powder printing. Constr Build Mater. 2019;217:394–402.
44. Jonat S, Hasenzahl S, Drechsler M, Albers P, Wagner KG, Schmidt PC. Investigation of compacted hydrophilic and hydrophobic colloidal silicon dioxides as glidants for pharmaceutical excipients. Powder Technol. 2004;141(1):31–43.
45. Kojima T, Elliott JA. Effect of silica nanoparticles on the bulk flow properties of fine cohesive powders. Chem Eng Sci. 2013;101:315–28.
46. Kim S, Bilgili E, Davé RN. Impact of altered hydrophobicity and reduced agglomeration on dissolution of micronized poorly water-soluble drug powders after dry coating. Int J Pharm. 2021;606:120853.
47. Chen L, Ding X, He Z, Fan S, Kunnath KT, Zheng K, Davé RN. Surface engineered excipients: II. Simultaneous milling and dry coating for preparation of fine-grade microcrystalline cellulose with enhanced properties. Int J Pharm. 2018;546(1):125–36.
48. Chen L, Ding X, He Z, Huang Z, Kunnath KT, Zheng K, Davé RN. Surface engineered excipients: I. improved functional properties of fine grade microcrystalline cellulose. Int J Pharm. 2018;536(1):127–37.
49. Chen L, He Z, Kunnath K, Zheng K, Kim S, Davé RN. Fine grade engineered microcrystalline cellulose excipients for direct compaction: assessing suitability of different dry coating processes. Eur J Pharm Sci. 2020;151:105408.
50. Chen L, He Z, Kunnath KT, Fan S, Wei Y, Ding X, Zheng K, Davé RN. Surface engineered excipients: III. Facilitating direct compaction tableting of binary blends containing fine cohesive poorly-compactable APIs. Int J Pharm. 2019;557:354–65.
51. Han X, Ghoroi C, Davé R. Dry coating of micronized API powders for improved dissolution of directly compacted tablets with high drug loading. Int J Pharm. 2013;442(1):74–85.
52. Giraud M, Gatumel C, Vaudez S, Bernard-Granger G, Nos J, Gervais T, Berthiaux H. Investigation of a granular bond number based rheological model for polydispersed particulate systems. Chem Eng Sci. 2020;228:16.
53. Massimilla L, Donsì G. Cohesive forces between particles of fluid-bed catalysts. Powder Technol. 1976;15(2):253–60.
54. Davé R, Kim S, Kunnath K, Tripathi S. A concise treatise on model-based enhancements of cohesive powder properties via dry particle coating. Advanced Powder Technology. 2022;33(11):103836.
55. Han X, Jallo L, To D, Ghoroi C, Davé R. Passivation of high-surface-energy sites of milled ibuprofen crystals via dry coating for reduced cohesion and improved flowability. J Pharm Sci. 2013b;102(7):2282–96.
56. Yu W, Hancock BC. Evaluation of dynamic image analysis for characterizing pharmaceutical excipient particles. Int J Pharm. 2008;361(1–2):150–7.
57. Yu W, Muteki K, Zhang L, Kim G. Prediction of Bulk Powder Flow Performance Using Comprehensive Particle Size and Particle Shape Distributions. Journal of Pharmaceutical Sciences. 2011;100(1):284–293.
58. Yu W, Liao L, Bharadwaj R, Hancock BC. What is the "typical" particle shape of active pharmaceutical ingredients? Powder Technol. 2017;313:7.
59. Freeman R. Measuring the flow properties of consolidated, conditioned and aerated powders — a comparative study using a powder rheometer and a rotational shear cell. Powder Technol. 2007;174(1):25–33.
60. Kim SS, C. Castillo, M. Sayedahmed, Dave RN. Reduced fine API agglomeration after dry coating for enhanced blend uniformity and processability of low drug loaded blends Pharm Res. 2022b;39:19.
61. Capece M, Silva KR, Sunkara D, Strong J, Gao P. On the relationship of inter-particle cohesiveness and bulk powder behavior: Flowability of pharmaceutical powders. Int J Pharm. 2016;511(1):178–89.